TANG, Rui; WANG, Shengwei; SHAN, Kui. Optimal and near-optimal indoor temperature and humidity controls for direct load control and proactive building demand response towards smart grids. Automation In Construction, 2018, 96: 250-261.

https://doi.org/10.1016/j.autcon.2018.09.020

Optimal and Near-Optimal Temperature and Humidity Controls for Direct Load Control and Proactive Building Demand Response towards Smart Grids

Rui Tang[1], Shengwei Wang[1,2*] and Kui Shan[1]

[1] Department of Building Services Engineering, The Hong Kong Polytechnic University, Kowloon, Hong Kong

[2] Research Institute for Sustainable Urban Development, The Hong Kong Polytechnic University, Kowloon, Hong Kong

Abstract: Shutting down part of operating chillers directly in central air-conditioning systems of buildings to meet the urgent demand reduction needs of power grids has received increasing attention recently. However, due to limited cooling supply during above demand response (DR) events, the indoor air temperature and particularly relative humidity would often increase to unacceptable levels, resulting in the failures of DR controls. Considering the restriction on power use during DR events, rational use of limited cooling supply turns out to be the inevitable choice. The feedback control strategies commonly-used today cannot properly deal with the environment and system control issues under limited cooling supply during DR events. However, no study on this problem can be found in the research literature. As the first effort, two control strategies (i.e., optimal and near-optimal) are developed to address the environment control issues (concerning both indoor temperature and humidity controls) under a pre-determined power limiting threshold during DR events. The optimal control strategy optimizes the air flow set-points of individual AHUs (air handling units) using model-based prediction and genetic algorithm to achieve the best possible indoor environment control. The near-optimal control strategy approaches such best environment control using a simple empirical method. Case studies are conducted and the results show that the air flow settings have significant impacts on the indoor environment controlled under limited cooling supply. Both control strategies can achieve significant improvements in the indoor temperature and humidity controls as well as significant fan power saving.

Keywords: temperature control, humidity control, fast demand response, direct load control, genetic algorithm, smart grid

1. Introduction

1.1 Background of research and related studies

The real-time balance between supply and demand sides of a power grid is a critical system requirement [1]. Any power imbalance will cause severe consequences in the reliability and quality of power supply (e.g. power outages, voltage fluctuations) [2]. The latest example happened in Australia in February 2017. Due to huge demand caused by the highest outdoor temperature in history, the power grid faced with a great challenge and failed. Facing the challenge from power imbalance, smart grid is considered as a state-of-the-art technology to incorporate advanced technologies to offer better flexibility, reliability and security in grid operation [3-5]. The power control at the consumer side in response to grid requests (e.g., dynamic price and reliability information) is known as demand response (DR). DR programmes cannot only benefit the operation of power grids but also offer economic benefits to end-users [6-10].

Buildings play an important role in DR programmes by actively altering their load profiles during peak times. Moreover, with the help of advanced technologies such as building automation systems and smart meters, demand response control strategies in buildings could be implemented to realize a bidirectional operation mode between buildings and power grids [11-13]. When pricing changes are informed day ahead or hours ahead, demand shifting achieved by rescheduling the system operation, such as resetting the indoor air temperature, is a preferable alternative to reduce the power demand of air-conditioning systems. Lee and Braun [14] proposed three simple approaches for estimating building zone temperature set-point variations to minimize the peak demand during critical demand periods considering the peak demand reduction. Sun et al. [15] developed a demand shifting control strategy including building load prediction, cooling charging and discharging controls to reduce the building peak demand. Su and Norford [16] modulated the power demand of a central air-conditioning system by adjusting the supply chilled water temperature and hence

the chiller power demand to satisfy the requirements of power grid. However, when adding an additional generation is extremely expensive or at the time of supply shortage, such conventional strategies are not sufficient to achieve significant demand reduction within a very short time, i.e., minutes, resulting from the inherent and significant delay of cooling charging and discharging control processes [17, 18].

In fact, the power demand of chillers accounts for a large part of power use in commercial buildings using central air-conditioning systems [19]. Shutting down some of operating chillers in an air-conditioning system, which is a typical fast demand response and direct load control method, would be effective for urgent requests of smart grids. Due to the effectiveness of this fast demand response method for the urgent requests of smart grids, many studies have been conducted. The authors of this paper [20] pointed out that imbalanced chilled water distribution among a central air-conditioning system occurred after simply shutting down some of operating chillers. A cooling distributor based on adaptive utility function was developed to deal with this problem. They [21] also proposed a novel control concept (i.e., supply-based feedback control strategy) for DR events, instead of conventional control strategies commonly used for central air-conditioning systems, to effectively avoid the serious operation problems (e.g., imbalanced cooling distribution) and ensure the expected immediate power reduction after adopting such fast demand response method. Simultaneously, such fast demand response method has been applied in real projects, such as by CLP, a major utility company in Hong Kong [22]. During DR period, the indoor environment would be considered. When a DR strategy of an air-conditioning system is adopted to benefit the smart grids, indoor thermal comfort would be potentially sacrificed to unacceptable levels [23]. Zhang et al. [24] investigated 56 subjects' thermal comfort during DR conditions and pointed out that subjects' thermal comfort zone during DR events was wider than that predicted by Fanger's PMV/PPD model. Chu et al. [25] developed a reasonable DR program with a least enthalpy estimator (LEE)-based fuzzy thermal comfort controller of

air-conditioning systems to control the fan-coil units. Results showed that the proposed method could ensure the indoor thermal comfort within the acceptable range. Although significant and immediate power reduction can be achieved by shutting down part of operating chillers, the indoor environment, particularly for the temperature and relative humidity, would be influenced obviously and thus essential to be considered.

1.2 Problem description and motivation of research

Currently, almost commonly-used automatic control strategies for central air-conditioning systems are demand-based feedback control. Such control logic can be managed properly in normal conditions when the total demand for each device is not more than the available cooling and all users can get what they need from their suppliers. However, when the cooling supply is not sufficient after part of operating chillers are simply shut down, the failure of conventional fan's control will occur. With limited cooling supply, the VAV dampers of indoor spaces would fully open and hence fans would operate at maximum speeds to maintain the original pressure set-points. The authors [26] pointed out such phenomenon (i.e., fully open VAV dampers and over-speeding fans) caused by the limited cooling supply using on-site measurements of a super-high commercial building. The excessive airflow circulated by full speeding of fans and cooled down by the limited cooling supply will lead to a serious increase of supply air temperature. Thus, the supply air with rather high temperature would almost lose the dehumidification ability. In the subtropical area such as Hong Kong, the humidity load in summer are always very high. In such a case, due to the unreasonable fan's control during DR events, not only the indoor air temperature (T) increases and deviates from the original set-point, but also the relative humidity (RH) would increase seriously, as shown in Fig.1. In normal conditions, the indoor air temperature is maintained at its set-point and RH fluctuates within an acceptable range. But during DR events (after shutting down part of operating

chillers), the indoor environment would be worse and the fans operate at their maximum speeds.

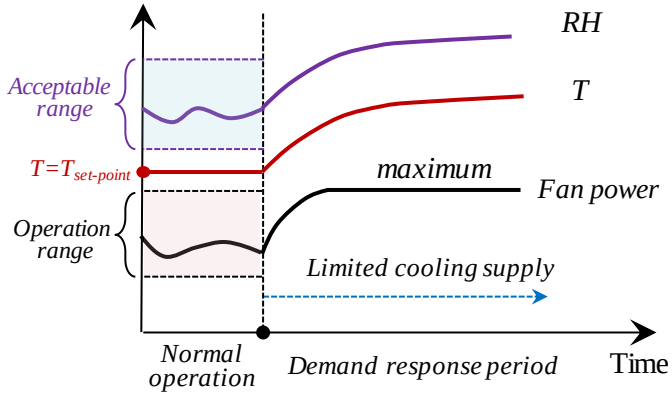

Fig.1 Indoor air temperature and relative humidity with limited cooling supply

In addition, much more power is consumed by the over speeding of fans and therefore potentially relieve the effect of DR control (i.e., power reduction). In fact, a pre-determined power reduction under a specific pricing incentive is signed ahead in the agreement with utility companies during a DR event [27]. In some mandatory incentive-based DR programmes, such as Interruptible/Curtailable (I/C) service, it is not economical and reasonable for end-users to prevent the unacceptable decrease of indoor thermal comfort at the expense of paying the penalty owing to unsatisfying the pre-determined power reduction. Therefore, under a pre-determined agreement on power use, rational use of limited cooling supply by optimizing the fan's control to achieve the best possible indoor environment would be a most effective and economical choice during DR events. This is the motivation of this study.

1.3 Outline of this research

This study, therefore, develops an online air flow optimization scheme to deal with above issues during DR events. The function of this scheme is realized by two strategies, a model-based optimal control strategy and an empirical near-optimal control strategy. The optimal control strategy is based on model-based prediction and genetic algorithm (GA) to modulate the air flow settings for individual AHUs (air handling units) during DR events. And the near-optimal control strategy achieves such

online optimization using an empirical method. Although this near-optimal strategy cannot obtain obviously good indoor environment as that using the optimal strategy, it is simple and convenient for applications and has no specific requirement on control facilities (as illustrated in §2.3). This study contributes three main innovations, including: (1) optimal control and near-optimal control strategies are developed for DR events taking the indoor humidity into account in addition to the indoor air temperature; (2) air flow settings for AHUs are optimized to improve the indoor environment during DR events under a pre-determined power limiting threshold; (3) two control strategies are developed to satisfy different primary needs of building owners, i.e., best possible indoor environment and simply practical applications. Case studies are conducted to test and validate the performance of these two proposed control strategies as well as to quantify the impacts of air flow settings on the indoor environment (temperature and relative humidity) during DR events.

2. Optimal and near-optimal control strategies for improved indoor temperature and humidity controls

During DR events, a pre-determined power reduction under a certain incentive should be achieved, which is signed ahead with utility companies in the agreement. With pre-defined power reduction and power demand baseline provided by utility companies, the power consumed by end-users should be maintained at a given power profile (i.e., power limiting threshold) during DR period accordingly. In this study, the contribution of the central air-conditioning system to a smart grid is considered, and the impacts of other parts on the building power demand are not considered.

Considering the impacts of air flowrate on indoor temperature and humidity (validated in §4.1), two effective methods are developed to optimize the setting of air flow for each AHU during a DR event in order to optimize the fan's control and hence improve the indoor environment in terms of indoor temperature and humidity.

2.1 Schematic of proactive fast demand response control strategy during DR events

The fast demand response strategy adopted in this study is shown in Fig.2. After part of operating chillers are shut down, the chiller load regulator is responsible to ensure the measured power demand follow the pre-determined power limiting threshold. With the predicted power limiting threshold and measured power demand, a PID controller followed by an amplification factor (K) is employed to realize the function of chiller load regulator. The control variable is the chilled water flow in the secondary loop representing the total cooling provided by chillers. The global cooling distributor is employed to properly distribute the available and limited cooling supply adjusted by the chiller load regulator among individual AHUs. Similarly, at the air-side, the online air flow optimization scheme is introduced to determine the set-points of total air flow of individual AHUs based on the actual measurements. The local cooling distributor is used to achieve proper air flow distribution (i.e., uniform indoor air temperature increase) among VAV (variable air volume) terminals associated to an AHU based on available air flowrate, i.e., flow set-point given by the online air flow optimization scheme. With optimized air flow delivered, the full speeding of fans can be effectively avoided. The chiller load regulator, (global and local) cooling distributors and prediction of power limiting threshold are developed in the previous study [28]. This study focuses on the online air flow optimization scheme, which aims at achieving optimal fan's control for a best possible indoor thermal comfort under a pre-determined power limiting threshold.

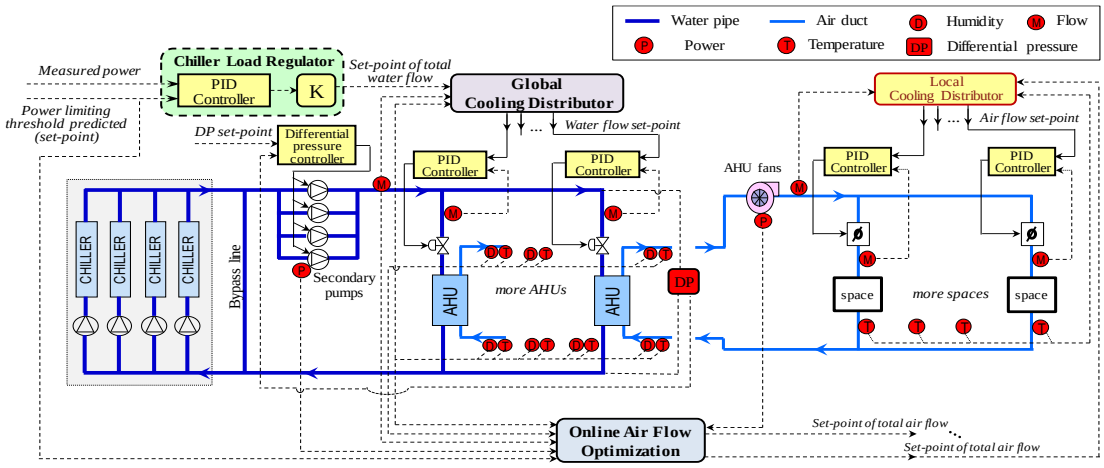

Fig.2 Schematic of proactive fast demand response control strategy during DR events

2.2 Optimal control strategy for online air flow optimization scheme

As for optimal control strategy, the online air flow optimization scheme is based on model-based prediction (explained in §2.2.1) and genetic algorithm optimization (explained in §2.2.2). It determines the optimal air flow set-points of individual AHUs in a building to minimize the indoor air temperature and maintain relative humidity of individual zones within an acceptable range. The schematic of online air flow optimization scheme is illustrated in Fig.3. At each sampling step, the GA optimizer starts with a set of random set-point trails within their allowed search ranges at their first generation. At the computation of each generation, the set of set-point trails is given to the model-based predictor. The predictor simulates the system thermal response within next prediction period, which is used by the fitness function to compute the fitness value. The GA optimizer then produces the next generation (another set of set-points trails) according to its rules and fitness value at current generation. Through sufficient generations of computation, the GA optimizer finds out the optimal set-point trails and they are eventually used to update the current set-points for process controller.

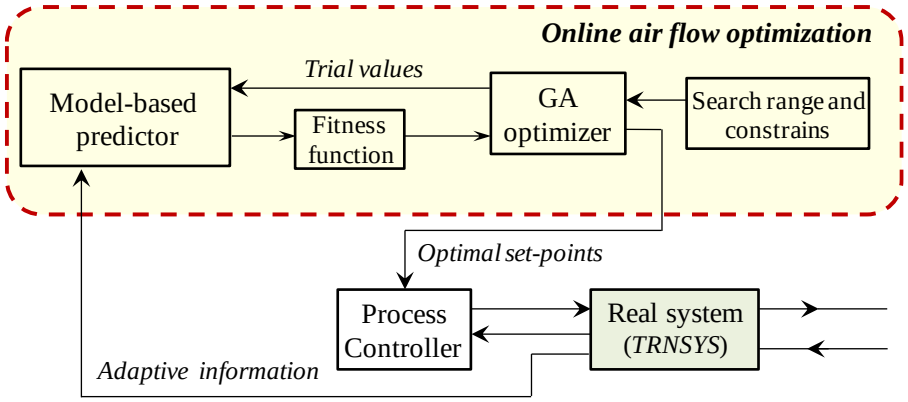

Fig.3 Schematic of online air flow optimization scheme

2.2.1 Description of models in the model-based predictor

Fan power model with self-correction

The power consumption of variable speed fans (P_{fan}, kW) depends on the

fan-delivered static pressure (Δp_{fan}, Pa), the air volume flow rate (V, m^3/s) and the efficiency (η), as shown in Eq.(1) [29]. The fan-delivered static pressure (Δp_{fan}) is determined by two components, as shown in Eq.(2). The first is the pressure head on the VAV air distribution system after the static pressure control sensor (p_{set}, Pa), which is a constant value in this study. The other component is the pressure loss across the rest of the VAV supply system, i.e., filters, coil, duct, etc., which is proportional to the square of the volume flow rate. The characteristic of efficiency is based on the manufacturers' data at the full speed operation and extended to the variable speed operation using the affinity law, as explained in Eq.(3) [30]. During a DR event, the supply air flow (V^k) is given by the GA optimizer.

$$P_{fan}^k = \frac{V^k * \Delta p_{fan}^k}{\eta^k} \quad (1)$$

$$\Delta p_{fan}^k = p_{set} + \gamma * (V^k)^2 \quad (2)$$

$$\eta^k = \eta_{design} * [d_0 + d_1 * x^k + d_2 * (x^k)^2 + d_3 * (x^k)^3] \quad (3)$$

where, η_{design} is the design fan efficiency. x^k is the fraction of nominal flow at *kth* time step during a DR event. d_0-d_3 and γ are the coefficients identified with the historic recorded data.

Considering the derivation existing between the prediction and real processes, the prediction model is further corrected in order to improve the accuracy by Eq.(4).

$$P_{fan}^k{}' = P_{fan}^k + e^{k-1} \quad (4)$$

where, $P_{fan}^k{}'$ is the predicted power consumption of fans at *kth* time step after correction, kW. e is the correction factor representing the estimated error between model perdition and real process, kW. At *(k-1)th* time step, the measurement of fan power consumption and state variable predicted by the model are compared to obtain the estimated error (e^{k-1}) for *kth* time step.

Total chilled water flow model with self-correction

The total chilled water flow (M_{tot}^k, kg/s) is realized by the module of chiller load

regulator, which is mainly based on PID algorithm through comparing the measured system power with the pre-determined power limiting threshold, as shown in Eq.(5). The discrete PID calculation is used to predict the output of PID controller in the module of chiller load regulator, as calculated by Eqs.(6-9). At *kth* time step, if a set of air flow settings is given, the power demand of fans (P_{fan}^{k}, kW) can be estimated by the fan power model. Then the system power can be predicted on basis of the predicted power demand of fans (P_{fan}^{k}) and the measured power demand of chillers and (primary & secondary) pumps (P_{cp}^{k}, kW). Accordingly, the difference (E^{k}) between the predicted system power and the pre-determined power limiting threshold is obtained, as calculated by Eq.(10).

$$M_{tot}^{k} = M_{tot,min} + U_{PID}^{k} * (M_{tot,max} - M_{tot,min}) \quad (5)$$

where, U_{PID}^{k} is the predicted output of PID controller in the module of chiller load regulator at *kth* time step. $M_{tot,max}$, $M_{tot,min}$ are the maximum and minimum mass water flow rates circulated in the secondary loop, which are pre-set in the model of amplification factor (K) in the chiller load regulator, kg/s.

$$U_{PID}^{k} = U_{P}^{k} + U_{I}^{k} + U_{D}^{k} \quad (6)$$

where, U_{P}^{k}, U_{I}^{k}, U_{D}^{k} are the proportional term, integral term and derivative term at *kth* time step, respectively.

$$U_{P}^{k} = K_{P} * E^{k} \quad (7)$$

$$U_{I}^{k} = \frac{K_{P}}{t_{I}} * \frac{(E^{k} + E^{k-1})}{2} * \Delta t_{s} + U_{I}^{k-1} \quad (8)$$

$$U_{D}^{k} = \frac{K_{P} * \frac{(E^{k} - E^{k-1})}{\Delta t_{S}} * t_{D} + U_{D}^{k-1}}{2} \quad (9)$$

where, K_{P}, t_{I}, t_{D} are the proportional, integral and derivative parameters of PID controller, respectively. Δt_{s} is the simulation time step of supervisory control, s.

$$E^{k} = P_{thr}^{k} - (P_{fan}^{k} + P_{cp}^{k}) \quad (10)$$

where, P_{thr}^{k} is pre-determined power limiting threshold during a DR event, kW. E^{k} is the difference between P_{thr}^{k} and predicted system power demand, kW.

Similar with the power model of fans, the model prediction is also further corrected in order to improve the accuracy, as shown in Eq.(11).

$$M_{tot}^{k}{}' = M_{tot}^{k} + e^{k-1} \tag{11}$$

where, $M_{tot}^{k}{}'$ is the predicted total chilled water flow at *kth* time step after correction, kg/s. *e* is the correction term representing the deviation between the model predictions and real processes, kg/s. At *(k-1)th* time step, the measurement of total chilled water flow and state variable predicted by the model are compared to obtain the estimated error (e^{k-1}) for *kth* time step.

Cooling distributor

After part of operating chillers are shut down, the cooling supply is not enough to satisfy the cooling demand of end-users. This would lead to the failure of conventional control strategies and hence limited cooling cannot be distributed properly [17]. Therefore, cooling distributors based on supply-based feedback control strategy are employed for cooling distributions in different level systems during DR events [18]. For the water-side of a central air-conditioning system, the global cooling distributor is used to distribute the total cooling supply (i.e., predicted total chilled water flow, $M_{tot}^{k}{}'$) among AHUs ($M_{sp,i}^{k}$, kg/s). Similar to the air-side, the local cooling distributor is used to distribute the air flow determined by the online air flow optimization scheme among VAV boxes associated with one AHU. The principle of global cooling distributor to predict the chilled water flow of individual AHUs is shown as an example in Eqs.(12-15).

$$U_{i}^{k} = 1 - \frac{\left|T_{i}^{k} - T_{set,i}\right|}{T_{band}} \qquad U_{i}^{k} \in [0,1] \tag{12}$$

where, T_{band} is a very large deviation between T_{i}^{k} (measured indoor air temperature, °C) and $T_{set,i}$ (original indoor set-point, °C), which should be large enough to fully cover the whole possible indoor temperature range of zones during a

DR event. Its value is set to be 10°C. U_i^k is the utility value, which is an economic concept applied in this allocation problem. a_i is a parameter representing the thermodynamic characteristics of i^{th} zone and calculation method is introduced in the reference.

$$M_{U=1,i}^k = M_{w,i}^k - \sqrt{\frac{1-U_i^k}{a_i}} \quad (13)$$

$$M_{U=1,i}^k = \lambda M_{U=1,i}^{k-1} + (1-\lambda) M_{U=1,i}^k \quad (14)$$

where, $M_{U=1,i}^k$ is the required chilled water flow of i^{th} zone to maintain the original utility value, that is, when the indoor air temperature is at its original set-point, kg/s. $M_{w,i}^k$ is the measured chilled water flow of i^{th} zone at *kth* time step, kg/s. Because the measurements always have obvious noise and fluctuation, a simple data filter is applied to update $M_{U=1,i}^k$ in order to fulfill the need of practical on-site applications, as shown in Eq.(14). λ is the forgetting factor selected to be 0.95 in this study.

$$M_{sp,i}^k = M_{U=1,i}^k + \sqrt{\frac{1-\bar{U}_{sp}^k}{a_i}} \quad (15)$$

where, $\bar{U}_{sp}^k$ is the target utility value of all zones at *kth* time step, which is the expected utility value of all zones if utility values of all zones are controlled to be the same. The value is determined based on the available cooling capacity (i.e., total chilled water flow, M_{tot}^k). $M_{sp,i}^k$ is the chilled water flow set-point for i^{th} zone at *kth* time step, kg/s.

AHU model

The function of the AHU (air handling unit) model is to calculate the temperature ($T_{a,out}$, °C) and humidity (G_{out}, kg) of the supply air. The classical number of transfer unit (NTU) and heat transfer effectiveness (ε) methods are applied to realize the heat transfer calculation. Two different methods are used for the heat conversion coefficient on the air side in dry and wet regions, respectively [31].

In the dry regime, the temperature and humidity of supply air are computed as follow:

$$NTU = \frac{UA}{C_{min}} = \frac{A}{C_{min}(R_a+R_m+R_w)} \quad (16)$$

$$\varepsilon = f(N_{row}, \frac{C_{min}}{C_{max}}, NTU) \quad (17)$$

$$Q = \varepsilon C_{min}(T_{in} - T_{w,in}) \quad (18)$$

$$T_{a,out} = T_{in} - \frac{Q}{C_p m_{air}} \quad (19)$$

$$G_{out} = G_{in} \quad (20)$$

where, A is the total heat transfer surface area, m^2. C_p is inlet air mass specific heat, kJ/(kg·K). C_{min}, C_{max} are the minimum and maximum capacity rates between air and water, kW/K. Q is the heat transfer occurred in AHU, kW. N_{row} is the number of the row. R_a, R_m and R_w are the heat transfer resistances of air side convection, coil metal and water side convection, which can be gained from manufactory's data, $(m^2K)/kW$. T_{in}, $T_{w,in}$ are the inlet air and water temperatures of AHU, °C. G_{in}, G_{out} are the inlet and outlet air humidity of AHU, kg. m_{air} is the mass flow rate of supply air, kg/s (i.e., trial value of air flow setting given by the GA optimizer, as shown in Fig.3).

In the wet regime, a fictitious air flow is assumed, which has a specific heat equal to the average saturation specific heat (c_s, specific heat of saturation moisture air at the average temperature of air inlet wet bulb temperature and water inlet temperature, kJ/(kg·K)). The air capacity flow rate (C_{af}, kW/K) and air convection coefficient of the fictitious air flow ($h_{a,wt}$, kJ/(kg·K)) are as follows:

$$C_{af} = m_{air} c_s \quad (21)$$

$$h_{a,wt} = h_a \frac{c_s}{c_p} \quad (22)$$

Then, the temperature and humidity of supply air are computed using the same approach:

$$NTU_f = \frac{UA}{C_{min,f}} = \frac{A}{C_{min,f}(R_{a,wt}+R_m+R_w)} \quad (23)$$

$$\varepsilon_f = f(N_{row}, \frac{C_{min,f}}{C_{max,f}}, NTU_f) \quad (24)$$

$$Q_{wt} = \varepsilon_f C_{min,f}(T_{in} - T_{w,in}) \quad (25)$$

$$T_{a,out} = T_{in} - \frac{SHR*Q_{wt}}{C_p m_{air}} \quad (26)$$

$$G_{out} = G_{in} - \frac{(1-SHR)*Q_{wt}}{H_{vap}} \quad (27)$$

where, *SHR* is the sensible heat ratio. *SHR* takes the same value calculated in the same inlet condition in the steady-state case using the bypass factor method. H_{vap} is water vaporization heat rate, kJ/(kg·s).

Adaptive dynamic building model

With predicted temperature and humidity of supply air and air flow rate for each zone, the indoor air temperature and humidity can be obtained as differential Eqs.(28-29) [32].

$$M_i c_p \frac{\partial T_{in}}{\partial t} = m_{air,i} c_p \left(T_{sup,i} - T_{in}\right) + Q_{s,i} \quad (28)$$

$$M_i \frac{\partial G_{in}}{\partial t} = m_{air,i} \left(G_{sup,i} - G_{in}\right) + D_i \quad (29)$$

where, M_i is the total mass of indoor air of i^{th} zone, kg. c_p is the specific heat of air, kJ/(kg · K). $T_{sup,i}$ and $G_{sup,i}$ are the temperature and humidity of supply air (i.e., $T_{a,out}$ and G_{out} calculated by AHU model). T_{in}, G_{in} are the indoor air temperature and humidity. $Q_{s,i}$, D_i are indoor heat (kW) and humidity loads (kg/s) of i^{th} zone.

Because of heat and humidity loads ($Q_{s,i}$, D_i) are slowly-varying variables, they are assumed to be constant during a very short period. Therefore, the Eqs.(28-29) can be expressed approximately as below by replacing the derivative terms approximately with finite difference terms. The indoor air temperature and humidity at *(k+1)th* time step can be predicted by Eqs.(30-31). Where, Δt_s is the time step of supervisory control. The superscript *k+1*, *k*, *k-1* are the last, current and next simulation time step of supervisory control, respectively.

$$T_{in}^{k+1} = T_{in}^{k} + \left[\frac{m_{air,i}^{k}}{M_i}\left(T_{sup,i}^{k} - T_{in}^{k}\right) + \frac{Q_{s,i}}{M_i c_p}\right]\Delta t_s \quad (30)$$

$$G_{in}^{k+1} = G_{in}^{k} + [\frac{m_{air,i}^{k}}{M_i}\left(G_{sup,i}^{k} - G_{in}^{k}\right) + \frac{D_i}{m_i c_p}]\Delta t_s \quad (31)$$

$$Q_{s,i}^{k} = M_i c_p \frac{T_{in}^{k} - T_{in}^{k-1}}{\Delta t_s} - \frac{m_{air,i}^{k-1} + m_{air,i}^{k}}{2} c_p (T_{sup,i}^{k-1} - T_{in}^{k-1}) \quad (32)$$

$$D_i^{k} = M_i c_p \frac{G_i^{k} - G_i^{k-1}}{\Delta t_s} - \frac{m_{air,i}^{k-1} + m_{air,i}^{k}}{2} (G_{sup,i}^{k-1} - G_{in}^{k-1}) \quad (33)$$

2.2.2 Optimization using genetic algorithm (GA)

Due to limited cooling supply during DR events, the cooling distributors are employed for the cooling distribution among different zones (one zone served by one AHU) in order to make sure indoor air temperatures of zones with the same temperature sacrifice (i.e., the increased value from the original set-point). Genetic algorithm (GA) is widely used in the optimization for the design and control of air-conditioning systems [33]. GA is a population-based stochastic global search technique inspired from the biological principles of natural selection and genetic recombination [34]. Each individual in the population, usually called chromosome, stands for a potential solution in the problem space. The chromosome is usually represented as a binary string which can capture both continuous and discrete variables. The fitness of an individual is related with its objective function value and it is used to determine the probability of each individual to be selected for reproduction. Then, crossover and mutation processes are applied on the selected individuals to produce a new population. The crossover process exchanges some genetic materials between two chromosomes, while the mutation process may flip the values of some bits at random. The above procedure is repeated until the maximum number of generations is reached.

In this study, the fitness function of GA optimizer is to minimize the average value of indoor air temperatures of all zones by identifying the optimal air flow settings of AHUs, as established in Eq.(34). The constraints for this optimization are shown in Eqs.(35-36).

$$min \quad \frac{1}{n}\sum_{i=1}^{n} T_{in}^{k+1} \quad (34)$$

$$\varphi_{in}^{k+1} \in [\varphi_{min,in}, \varphi_{max,in}] \quad (35)$$

$$V_{set,i}^{k+1} \in [0.7y_i, 1.3y_i] \quad (36)$$

where, T_{in}^{k+1} and φ_{in}^{k+1} are the indoor air temperature and relative humidity of i^{th} zone at $(k+1)th$ time step. $\varphi_{min,in}$ and $\varphi_{max,in}$ are the lower and upper limits of acceptable indoor relative humidity. $V_{set,i}^{k+1}$ is the set-point of air flow for i^{th} zone at $(k+1)th$ time step, which is the optimal setting, kg/s. y_i is the air flow of i^{th} zone just before the DR event, kg/s. The set-point, $V_{set,i}^{k+1}$, is in the range between ±30% of that right before the DR event. If more air flow is delivered, the original supply static pressure set-point may not meet the requirement, while too little air flow may result in insufficient fresh air during DR events. The genetic algorithm is used to search for the optimal values of variables (i.e., air flow set-points, $V_{set,i}^{k+1}$) that minimize the fitness function.

2.3 Near-optimal control strategy for online air flow optimization scheme

The main difference between the optimal and near-optimal control strategy is the requirement of the control facility. The above optimal control strategy can find out the best possible solutions but the prediction and optimization (using GA) processes should be achieved with the help of personal computers (PC). When building automation systems (BAS) are only employed with the direct digital controller (DDC) and only some simple control logic can be implemented, a near-optimal control strategy using an empirical method is therefore developed. Undoubtedly, the indoor environment optimized by this near-optimal strategy would be not obviously good as that using the optimal control strategy. But this simple strategy is no specific requirement for the control facilities and accordingly convenient to be implemented for DDC directly in real applications.

The near-optimal control strategy optimizes the air flow settings of AHUs based on an empirical method. Generally, the air flow of each fan would decrease for the balance of power demands between water and air sides of an air-conditioning system when system total power demand is limited during a DR event. The design air flows and system rated power demand are considered as a reference and the air flow setting

417 of a zone during a DR event is proportional to its design value based on the ratio
418 between given power limiting threshold and system rated power demand, as shown in
419 Eq.(37).

420 $$V_{set,i} = (\frac{P_{DR}}{P_{rated}}) \times V_{design,i} \quad (37)$$

421 where, $V_{set,i}$ is the air flow setting of i^{th} zone. These settings are unchanged during
422 an entire DR event. $V_{design,i}$ is the design air flow of i^{th} zone. P_{DR} is the average of
423 power limiting threshold profile during the DR event. P_{rated} is rated power demand
424 of an air-conditioning system including chillers, pumps and fans.

425 **3. Test platform**

426 Computer-based simulation is an effective means to test and validate the proposed
427 control strategy in this study. A virtual simulation platform is built to simulate a
428 high-rise commercial building integrated with a smart grid using dynamic models
429 developed on TRNSYS [35]. This simulation platform employs detailed physical
430 models including the building envelope and major components (e.g. chillers, pumps,
431 fans, hydraulic network, air ducts, AHUs) of a central air-conditioning system. The
432 dynamic processes of heat transfer, hydraulic characteristics, water flow and air flow
433 balance schemes, energy conservation and controls among the whole system are
434 simulated. The GA is programmed by MATLAB and used to attain the optimal control
435 signals through the existing interface Type 155 on TRNSYS. Three important
436 parameters including "PopulationSize", "TolFun" and "Generations" are assigned
437 with the values of 50, 1×10^{-6} and 200, respectively. The parameter "PopulationSize"
438 indicates the number of individuals; "TolFun" is the termination tolerance; and
439 "Generations" represents the maximum number of generations.

440 The central chiller plant concerned in this study is a typical primary
441 constant-secondary variable chilled water system. It consists of four identical chillers
442 with rated capacity of 4080 kW, four primary pumps and four secondary water pumps.
443 Each chiller is associated with a primary chilled water pump of constant speed (172.5

L/s). Six air-conditioned zones with different cooling load profiles cooled by six AHUs are selected to illustrate the problems to be solved and to test the proposed control strategies as well. The areas of the six zones are 1600m^2, 1600m^2, 1600m^2, 2400m^2, 1200m^2, and 1600m^2 respectively. The ceiling height of each zone is 3.5 m. The window-to-wall ratio is 0.5. Each AHU is equipped with one supply and one return air delivery fans. The fresh air flow set-point of the AHU is set at a constant value according to the ASHRAE Standard 62.1-2013. The original indoor air temperature set-point in normal condition is set to be 24℃. The office hour of the building is between 08:00AM and 18:00PM and the DR period is set to be two hours between 14:00PM and 16:00PM in a typical summer day in Hong Kong. The outdoor weather condition of the test day is shown in Fig.4. During DR events, shutting down part of operating chillers is adopted to provide immediate power reduction responding to urgent requests of smart grids.

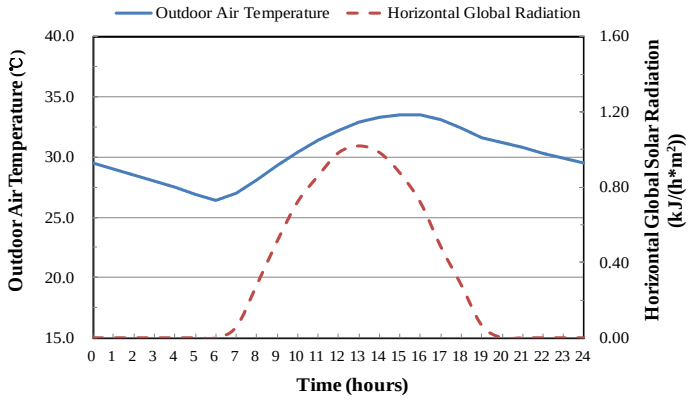

Fig.4 Outdoor dry-bulb temperature and solar radiation in the test day

The power baseline profile and the corresponding power limiting threshold profile for the building during the DR event including four parts, i.e., chillers, primary pumps, secondary pumps and air delivery fans, are shown in Fig.5. The power limiting threshold is given considering the indoor air temperature limit (i.e., 27^{o}C) during the DR event [28]. For the power rebound (PR) period, the air flow settings in these two proposed control strategies maintain the same as the values right before the DR event till the indoor air temperatures recover to the set-points in normal conditions.

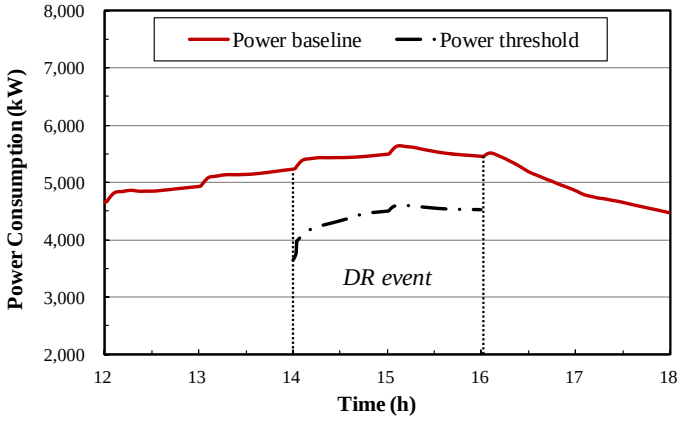

Fig.5 Baseline profile and power limiting threshold during a DR event

At the start of the DR event, one of four operating chillers, one of four primary pumps and two of four secondary pumps are shut down. In the simulation tests, the sampling interval of online air flow optimization scheme using optimal control strategy is 60 seconds. The sampling intervals of the cooling distributors/load regulator and simulation time step are 1 second.

4. Test and Validation

4.1 Impacts of air flowrate on indoor air temperature and humidity

In this session, tests to investigate the impacts of air flow setting on the indoor air temperature and relative humidity were conducted when the power consumption of the building was maintained at a pre-determined power limiting threshold during a DR event. Seven case studies were conducted. The values of air flow rates of individual zones right before the DR event were considered as the reference when changing the air flow settings. In addition to the reference case, tests under six different air flow rates of all AHUs (zones) were conducted, including: -45% (reduced by 45% from reference case), -30%, -15%, +15% (increased by 15% from reference case), +30%, +45% and +60%.

Fig.6 presents the average and maximum values of indoor air temperature and relative humidity under different air flow settings. The temperature and relative humidity in a zone were represented by the return air temperature and relative

humidity of the zone (AHU). The average/maximum indoor air temperatures and relative humidity presented were the corresponding values of the averages of six zones during the secondary hour of the DR event (i.e., the critical period). As the air flow increased, the (average and maximum) indoor air temperatures first rose and then decreased while the opposite tendencies happened to the relative humidity. In the reference case, the average indoor air temperature and relative humidity were about 26.9°C and 64%, respectively. If the air flow obviously decreased (to -45%), the indoor temperature would increase. More power consumed by water-side of the air-conditioning system to provide more cooling but the less air flow caused by the decrease of power demand of fans could not deliver cooling supply completely, as shown in Fig.7. Moreover, the relative humidity also experienced a slight decrease mainly caused by the indoor temperature increase.

By contrast, when much more air flow was delivered as the condition of the DR event (caused by the full speeding of fans), the cooling provided by water-side was decreased seriously and hence the indoor temperature increased significantly although excessive air flow was circulated. The rates of cooling supply decrease and indoor temperature increase went up along with the air flow increased because of the third-order relationship between fan power and its air flow delivered. For the relative humidity, the high supply air temperature caused by the excessive air flow and limited cooling supply would potentially reach the level almost lost the dehumidification ability. When the indoor humidity load was very high and not effectively removed by the supply air, the relative humidity would seriously increase until the increase rate of indoor temperature exceeded the humidity load increase. In Fig.6, after the air flow increased by 30%, the maximum indoor temperature reached 29℃ (i.e., more than 2℃ increase) and the maximum relative humidity approached to the peak (i.e., over 80%). Then, the relative humidity began to decrease considering the fact that almost no cooling could be provided and the indoor temperature seriously increased.

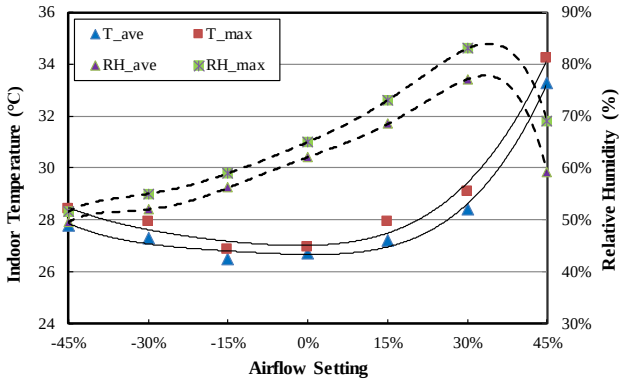

514

515 Fig.6 Average and maximum values of indoor air temperatures and relative humidity

516 during a DR event – under a pre-determined power limiting threshold

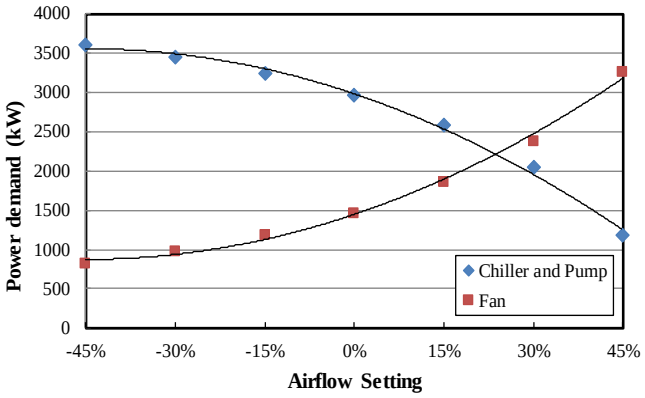

517

518 Fig.7 Power demands of chillers, pumps and fans during a DR event – under a

519 pre-determined power limiting threshold

520 Overall, with a determined total power demand, the higher power consumption

521 of air delivery fans (i.e., air-side) for providing more air flow would reduce the power

522 consumption of chilled water system (i.e., water-side) and cooling supply. The

523 reduced cooling supply but massive air flow would lead to the temperature increase of

524 supply air and also exacerbate the decrease of dehumidification ability of supply air. It

525 is worthy of noticing that the setting of air flow rate for each AHU has obvious

526 impacts on indoor air temperature and relative humidity. A higher or lower air flow

527 setting is not an optimal selection for the indoor environment under a pre-determined

528 power limiting threshold. There exists a best possible indoor environment realized by

529 the air flow settings during a DR event.

4.2 *Validation of proposed optimal and near-optimal control strategies*

In this session, the indoor air temperatures and relative humidity in three cases are presented with different strategies for air flow settings of AHUs during the DR event, including: conventional feedback control strategy (i.e., reference case), near-optimal control strategy and optimal control strategy.

Reference case – under conventional feedback control strategy during a DR event

If using the conventional feedback control strategy in the condition of limited cooling supply, the fans would be fully operating to maintain the original static pressure set-points because of fully opened VAV dampers. Although maximum air flows were delivered to individual zones, not only the indoor air temperatures and the relative humidity increased significantly but also the power consumption of the air-conditioning system obviously increased and even relieved the effect of DR controls (i.e., power reduction, as shown in Fig.14). As shown in Fig.8, the indoor air temperatures of all zones approached to 28℃ during the DR period, and relative humidity was over 80% (increasing about 20% compared with that right before the DR event). In addition to the unacceptable indoor environment, the system power consumption during the DR period did not reduce and was even higher than the original profile without a DR control (i.e., baseline). Therefore, it is important to adopt alterative control to avoid such poor operation and control in DR events.

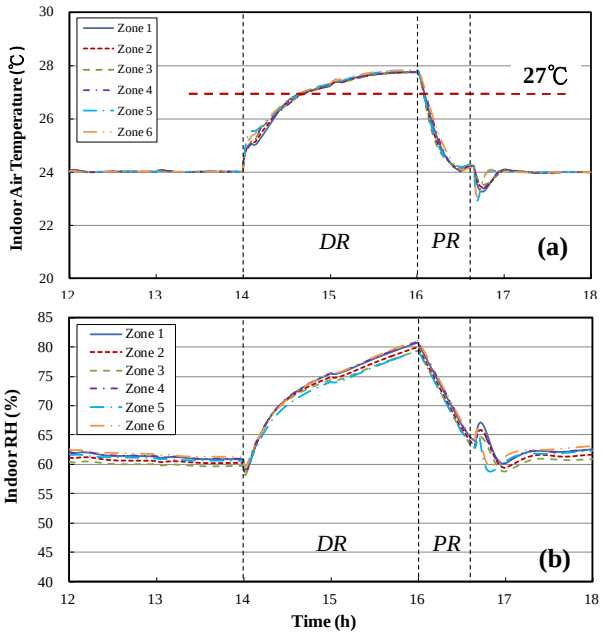

Fig.8 Indoor air temperature (a) and relative humidity (b) profiles of individual zones during a DR event – under conventional feedback control strategy

Near-optimal control strategy – under empirical air flow settings during a DR event

In this case, the settings of air delivery fans during DR events were maintained at constant values determined by the near-optimal control strategy. Such empirical setting could avoid unreasonable environment control and speeding of fans and also simplify the optimization process but it cannot achieve a best possible indoor environment.

Fig.9 presents the indoor air temperature and relative humidity profiles of all six zones, represented by that of return air of individual AHUs, during the DR event. The indoor environment was obviously better than that in the reference case. The indoor air temperatures of all six zones were below 27℃, and relative humidity was much lower than that in the reference case (i.e. only increased slightly in the DR event, below 65%). Fig.10 presents the air flow rate of individual zones determined by the near-optimal control strategy. The air flow rates of individual AHUs were set as constant using the near-optimal control strategy to avoid massive air flows circulated in AHUs during the DR event.

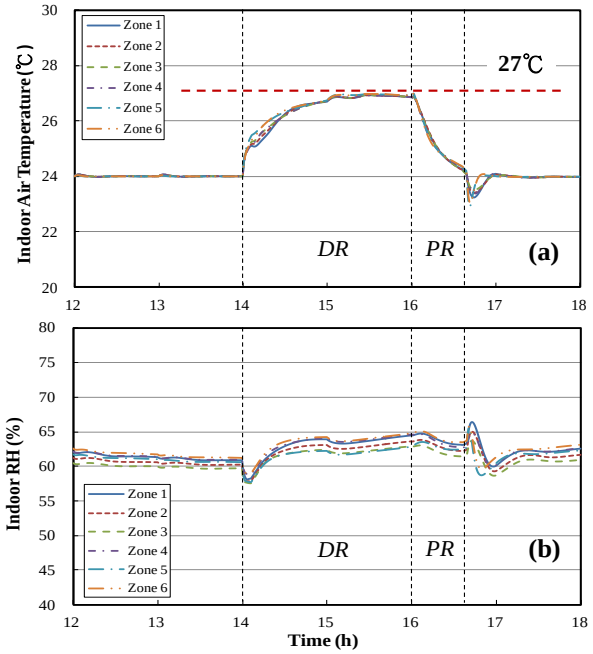

Fig.9 Indoor air temperature (a) and relative humidity (b) profiles of individual zones during a DR event – under near-optimal control strategy

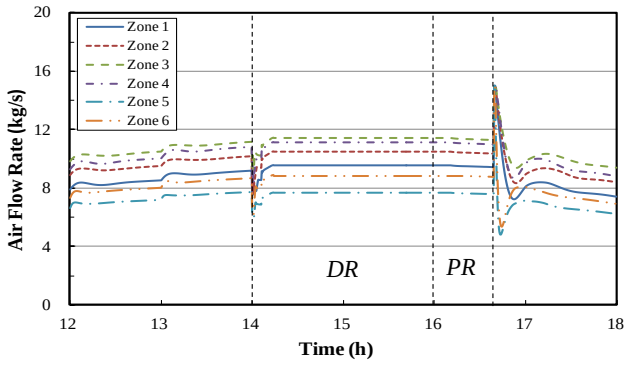

Fig.10 Air flow rate of individual zones during a DR event – under near-optimal control strategy

Optimal control strategy – under optimal air flow settings during a DR event

Using the proposed optimal control strategy, the profiles of indoor air temperature and relative humidity during the DR event are shown in Fig.11. With the optimal air flow settings, the indoor air temperature of each zone during the critical period of DR event fluctuated around 26.3℃, which was significantly improved in comparison to the reference case (i.e., decreased for nearly 1.5℃) and the near-optimal case (i.e., decreased for about 0.8℃). Moreover, the indoor relative humidity of zones with

optimal settings was significantly improved compared with the reference case (reduced from about 80% to less than 60%) and obviously lower than that using near-optimal strategy (reduced from about 65% to less than 60%) during the DR event. In fact, the indoor relative humidity of zones with optimal settings did not increase but slightly decreased compared with that right before the DR event.

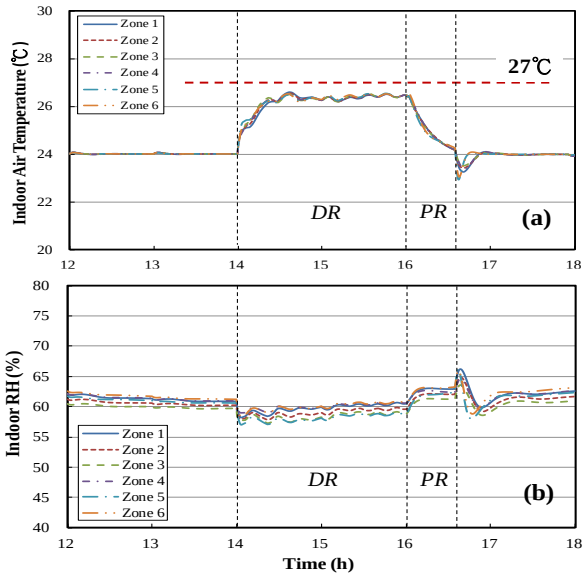

Fig.11 Indoor air temperature (a) and relative humidity (b) profiles of individual zones during a DR event – under optimal control strategy

The air flow rates of zones determined by the optimal control strategy during the DR event are shown in Fig.12. Compared with the values used for the near-optimal control strategy, the air flows of zones were varying to achieve a better indoor environment during the DR period. During the power rebound (PR) period, the air flows for zones were set to be nearly the same as that of the corresponding zones right before the DR event in order to avoid the overspending of fans. Such air flow settings were used until the indoor air temperatures reached their original set-points and PR period ended.

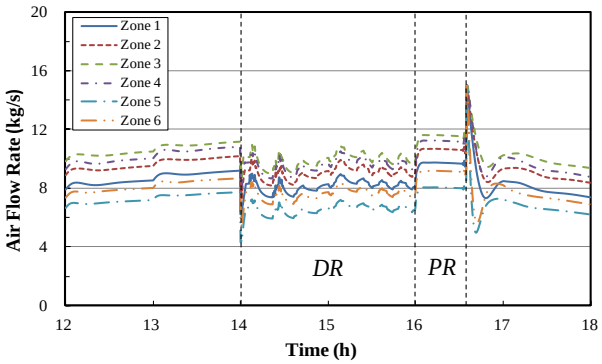

Fig.12 Air flow rates of individual zones during a DR event – under optimal control strategy

Fig.13 presents the comparison of the temperature and dehumidification ability of supply air among these three cases. The dehumidification refers to the removed humidity load by the AHU. Using the conventional control strategy in the reference case, the failure of fans' control resulted in excessive air flow circulated in each AHU. As a result, the supply air temperature was rather high (over 20°C) and the dehumidification ability was almost lost (near to zero). Although much more power was consumed and even relieved the effect of the DR control, the indoor temperature and relative humidity were rather bad. But with optimal and near-optimal control strategies, the air flows delivered by fans were effectively controlled/optimized and the supply air temperature significantly decreased. Then the dehumidification ability of supply air had significant improvements particularly using optimal control strategies, which the removed humidity load was nearly equal to the level in normal condition.

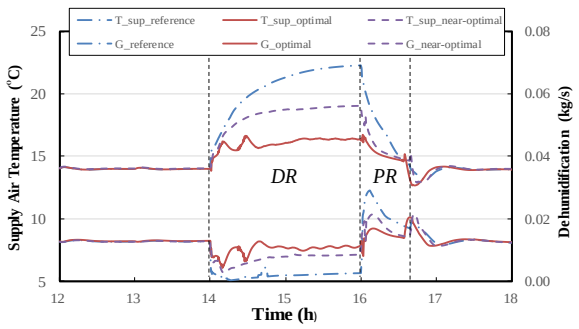

Fig.13 Temperature and dehumidification ability of supply air among three cases during a DR event

615 The comparison of indoor air temperature and relative humidity among these three
616 cases is shown in Table 1. In general, using the near-optimal and optimal control
617 strategies, the indoor air temperatures and relative humidity were significantly
618 improved during the DR event. Compared with the reference case, the near-optimal
619 strategy could reduce the average and maximum indoor air temperatures about 0.8°C
620 and 1°C respectively. The average and maximum relative humidity were both
621 improved about 15% during the DR event. Using the optimal control strategy, both
622 the average/maximum temperatures were improved nearly 1.5°C and the
623 average/maximum indoor relative humidity reduced about 20% in comparison to that
624 in the reference case. The optimal control strategy also achieved over 0.5°C reduction
625 in average indoor air temperature and about 5% reduction in relative humidity
626 compared with that using the near-optimal strategy. It is worthy of noticing that with
627 the optimal control strategy, the reduction of average indoor air temperature during
628 the DR event exceeded the threshold of human perception of temperature difference
629 (i.e., 0.5°C). Moreover, the indoor relative humidity was also improved although it
630 was not so much, less than 5%. Therefore, using optimal control strategy, the
631 occupants could perceive the improvement of indoor thermal comfort, particularly for
632 the indoor air temperature. It can be also found that near-optimal strategy is a
633 convenient means, which can achieve reasonably good indoor environment and fan
634 controls.

635 Table 1 Comparison of three cases on indoor air temperature and relative humidity

		Reference case	Near-optimal control strategy	Optimal control strategy
Temperature increased	Average (°C)	27.65	26.88	26.34
	Improved (K)		0.77	1.31
	Max (°C)	27.91	26.98	26.54
	Improved (K)		0.93	1.37
Relative humidity	Average (%)	77.51	63.19	59.64
	Improved (%)		14.32	17.87
	Max (%)	81.12	64.81	60.87
	Improved (%)		16.31	20.25

The power demands of the air-conditioning system using the near-optimal and optimal control strategies are shown in Fig.14. Using the conventional control strategy during the DR event, the system power demand almost relieved the effect of the DR control and even exceeded the baseline profile because of the significant increase of power consumption of air delivery fans. The near-optimal and optimal control strategies could effectively ensure the system power demand well follow the pre-determined power limiting threshold during the DR event. During the DR event, the average power demand was reduced approximately from 6000kW to 4500kW, about 25%, and meanwhile ensured the indoor environment using the proposed control strategies. It was worthy of noticing that the indoor environment (i.e., temperature and relative humidity) could be obviously improved by optimizing the air flow settings for individual AHU fans without extra power demand required. Hence, these two proposed control strategies not only ensure an acceptable indoor environment, but also explore the potential of power reduction for the benefits of building owners (in terms of cost saving) and the smart grids (in terms of grid power balance and overall grid efficiency).

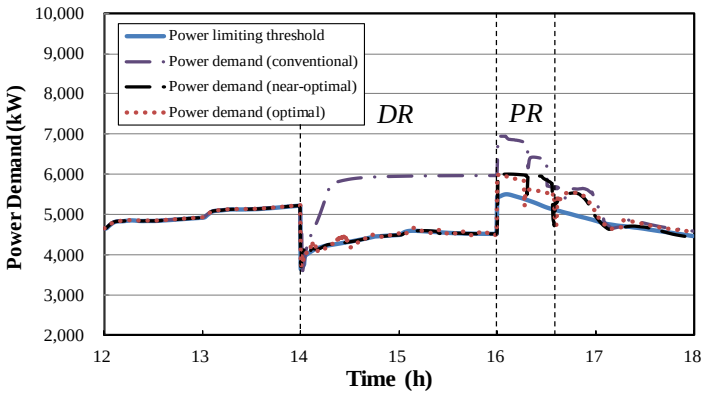

Fig.14 Power demands of air-conditioning system during a DR event under different control strategies

5. Conclusions

In the condition of limited cooling supply during DR events, indoor air temperature and relative humidity would potentially increase and even to

658 unacceptable levels, while the conventional feedback controls commonly used today
659 for indoor environment and air-side systems cannot effectively use the limited cooling
660 supply to achieve proper indoor environment control. Therefore, an online air flow
661 optimization scheme is developed for the controls of indoor environment and air-side
662 system during direct load control or fast demand response events. Two strategies are
663 proposed for this scheme, optimal control strategy and near-optimal control strategy,
664 in order to meet the different requirements in real applications. The optimal control
665 strategy, which is based on model-based prediction and genetic algorithm (GA)
666 optimization, can adjust air flow set-points of individual AHUs properly to achieve
667 the best possible indoor environment (i.e., temperature and relative humidity) under
668 limited cooling supply and pre-determined power limiting threshold. The near-optimal
669 control strategy can approach such best environment control using a simple empirical
670 method, which is very convenient to be implemented in engineering practice.
671 Test results also show that the air flow settings of AHUs have significant impacts
672 on the indoor air temperature and relative humidity under limited cooling supply and
673 under pre-determined power limiting threshold. With the conventional feedback
674 control strategy during DR events, the indoor temperature and relative humidity
675 increase seriously while the system power demand might not reduce effectively due to
676 the over-speeding of fans. Using the proposed near-optimal and optimal control
677 strategies, the average indoor air temperatures reduced about 0.77^{o}C and 1.31^{o}C
678 during the DR event, while the maximum relative humidity reduced more than 16%
679 and 20%, respectively. Moreover, the power demands of the air-conditioning system
680 can be well controlled below the pre-determined power limiting threshold. These two
681 proposed control strategies can improve the indoor thermal comfort effectively and
682 ensure the success of the DR controls. At the same time, the proposed strategies
683 provide the possibility to achieve more power reduction during DR events (given by
684 significantly reduced fan power demand).

Application issue: the proposed control strategies effectively solve the system control and indoor environment control (i.e., indoor temperature and relative humidity) problems for central air-conditioning systems when shutting down part of operating chillers is adopted as a fast demand response method for urgent requests of smart grids. Meanwhile, the pre-determined power reduction signed ahead with utility companies can be ensured.

The proposed control strategies have a wide application and are not limited to some certain areas/conditions. The system control and indoor environment control problems occurred during fast DR events are caused by the inherent system control logic of conventional strategies, which is based on the assumption that the total cooling supply is sufficient. The limited cooling supply after shutting down part of operating chillers leads to the failure of commonly-used control strategies and hence results in the system operation problems. The indoor air temperature will increase and fans are out of control. For the areas/conditions with low humidity load (e.g., dry outdoor weather conditions), indoor relative humidity is not a critical problem because of the increased indoor temperature. By contrast, for the areas/conditions with high humidity load, the reduced dehumidification ability of supply air would lead to the indoor relative humidity increase and even to unacceptable levels.

6. Acknowledgements

The research presented in this paper is financially supported by a grant (152152/15E) of the Research Grant Council (RGC) of the Hong Kong SAR and a grant under the Strategic Focus Area (SFA) Scheme of the Research Institute for Sustainable Urban Development (RISUD) in The Hong Kong Polytechnic University.

Reference

[1] Agency IE. IEA Statistics: World energy statistic and balances. Organisation for Economic Co-operation and Development. International Energy Agency. 2014. https://www.iea.org/publications/freepublications/publication/KeyWorld2014.pdf. (last viewed date: July 2, 2018).

[2] R.N. Allan. Reliability evaluation of power systems. Springer Science & Business Media, 2013. ISBN 978-1-4899-1860-4.
[3] J. Yuan, Z. Hu. Low carbon electricity development in China - an IRSP perspective based on super smart grid. Renewable and Sustainable Energy Reviews 15 (6) (2011) 2707-2713. https://doi.org/10.1016/j.rser.2011.02.033.
[4] M. Azzi, H. Duc, Q. Ha. Toward sustainable energy usage in the power generation and construction sectors - a case study of Australia. Automation in Construction 59 (2015) 122-127. https://doi.org/10.1016/j.autcon.2015.08.001.
[5] M.P. Moghaddam, A. Abdollahi, M. Rashidinejad. Flexible demand response programs modeling in competitive electricity markets. Applied Energy 88 (9) (2011) 3257-3269. https://doi.org/10.1016/j.apenergy.2011.02.039.
[6] P. Pinson, H. Madsen. Benefits and challenges of electrical demand response: A critical review. Renewable and Sustainable Energy Reviews 39 (2014) 686-699. https://doi.org/10.1016/j.rser.2014.07.098.
[7] M.H. Albadi, E.F. El-Saadany. A summary of demand response in electricity markets. Electric Power Systems Research 78 (11) (2008) 1989-1996. https://doi.org/10.1016/j.epsr.2008.04.002.
[8] K.M. Tsui, S.C. Chan. Demand response optimization for smart home scheduling under real-time pricing. IEEE Transactions on Smart Grid 3 (4) (2012) 1812-1821. DOI: 10.1109/TSG.2012.2218835.
[9] T.M. Lawrence, M.C. Boudreau, L. Helsen, G. Henze, J. Mohammadpour, D. Noonan, D. Patteeuw, S. Pless, R.T. Watson. Ten questions concerning integrating smart buildings into the smart grid. Building and Environment 108 (2016) 273-283. https://doi.org/10.1016/j.buildenv.2016.08.022.
[10] F. Rahimi, A. Ipakchi. Demand response as a market resource under the smart grid paradigm. IEEE Transactions on Smart Grid 1 (1) (2010) 82-88. DOI: 10.1109/TSG.2010.2045906.
[11] P. Siano. Demand response and smart grids—A survey. Renewable and Sustainable Energy Reviews 30 (2014) 461-478. https://doi.org/10.1016/j.rser.2013.10.022.
[12] S.S.S.R. Depuru, L. Wang, V. Devabhaktuni. Smart meters for power grid: Challenges, issues, advantages and status. Renewable and Sustainable Energy Reviews 15 (6) (2011) 2736-2742. https://doi.org/10.1016/j.rser.2011.02.039.
[13] K. Klein, S. Herkel, H.M. Henning, C. Felsmann. Load shifting using the heating and cooling system of an office building: Quantitative potential evaluation for different flexibility and storage options. Applied Energy 203 (2017) 917-937. https://doi.org/10.1016/j.apenergy.2017.06.073.
[14] K.H. Lee, J.E. Braun. Development of methods for determining demand-limiting setpoint trajectories in buildings using short-term measurements. Building and Environment 43 (10) (2008) 1755-1768. https://doi.org/10.1016/j.buildenv.2007.11.004.
[15] Y.J. Sun, S.W. Wang, G.S. Huang. A demand limiting strategy for maximizing

monthly cost savings of commercial buildings. Energy and Buildings. 42 (2010) 2219-2230. https://doi.org/10.1016/j.enbuild.2010.07.018.

[16] L. Su, L.K. Norford. Demonstration of HVAC chiller control for power grid frequency regulation - Part 1: Controller development and experimental results. Science and Technology for the Built Environment 21 (8) (2015) 1134-1142. https://doi.org/10.1080/23744731.2015.1072449.

[17] S.W. Wang, D.C. Gao, R. Tang, F. Xiao. Cooling supply-based HVAC system control for fast demand response of buildings to urgent requests of smart grids. Energy Procedia 103 (2016) 34-39. https://doi.org/10.1016/j.egypro.2016.11.245.

[18] S. Nolan, M. O'Malley. Challenges and barriers to demand response deploy ment and evaluation. Applied Energy 152 (2015) 1-10. https://doi.org/10.1016/j.apenergy.2015.04.083.

[19] L. Pérez-Lombard, J. Ortiz, C. Pout. A review on buildings energy consumption information. Energy and Buildings 40 (3) (2008) 394-398. https://doi.org/10.1016/j.enbuild.2007.03.007.

[20] R. Tang, S.W. Wang, D.C. Gao, K. Shan. A power limiting control strategy based on adaptive utility function for fast demand response of buildings in smart grids. Science and Technology for the Built Environment 22 (6) (2016) 810-819. https://doi.org/10.1080/23744731.2016.1198214.

[21] S.W. Wang, R. Tang. Supply-based feedback control strategy of air-conditioning systems for direct load control of buildings responding to urgent requests of smart grids. Applied Energy 201 (2017) 419-432. https://doi.org/10.1016/j.apenergy.2016.10.067.

[22] CLP. CLP information kit. 2014. https://www.clp.com.hk/en/about-clp-site/corporate-information-site/scheme-of-control-site/Documents/4.1%20CLP%20Information%20Kit.pdf. (last viewed date: July 2, 2018).

[23] F. Zhang, R. de Dear. Application of Taguchi method in optimising thermal comfort and cognitive performance during direct load control events. Building and Environment 111 (2017) 160-168. https://doi.org/10.1016/j.buildenv.2016.11.012.

[24] F. Zhang, R. de Dear, C. Candido. Thermal comfort during temperature cycles induced by direct load control strategies of peak electricity demand management. Building and Environment 103 (2016) 9-20. https://doi.org/10.1016/j.buildenv.2016.03.020.

[25] C.M. Chu, T.L. Jong, Y.W. Huang. A direct load control of air-conditioning loads with thermal comfort control. Power Engineering Society General Meeting (2005) 664-669. DOI: 10.1109/PES.2005.1489078.

[26] R. Tang, S.W. Wang, K. Shan, H. Cheung. Optimal control strategy of central air-conditioning systems of buildings at morning start period for enhanced energy efficiency and peak demand limiting, Energy 151 (2018) 771-781. https://doi.org/10.1016/j.energy.2018.03.032.

[27] P. Palensky, D. Dietrich. Demand side management: Demand response, intelligent

energy systems, and smart loads. IEEE transactions on industrial informatics 7(3) 2011 381-388. DOI: 10.1109/TII.2011.2158841.

[28] R. Tang, S.W. Wang, C.C. Yan. A direct load control strategy of centralized air-conditioning systems for building fast demand response to urgent requests of smart grids. Automation in Construction 87 (2018) 74-83. https://doi.org/10.1016/j.autcon.2017.12.012.

[29] S.W. Wang, J. Burnett. Variable-air-volume air-conditioning systems: Optimal reset of static pressure setpoint. Building Services Engineering Research and Technology 19 (4) (1998) 219-231.https://doi.org/10.1177/014362449801900406.

[30] S.W. Wang, J. Burnett. Online adaptive control for optimizing variable-speed pumps of indirect water-cooled chilling systems. Applied Thermal Engineering 21 (11) (2001) 1083-1103. https://doi.org/10.1016/S1359-4311(00)00109-5.

[31] S.W. Wang. Dynamic simulation of a building central chilling system and evaluation of EMCS on-line control strategies. Building and Environment 33 (1) (1998) 1-20. https://doi.org/10.1016/S0360-1323(97)00019-X.

[32] S.W. Wang. Dynamic simulation of building VAV air-conditioning system and evaluation of EMCS on-line control strategies. Building and Environment 34 (6) (1999) 681-705. https://doi.org/10.1016/S0360-1323(98)00052-3.

[33] L.G. Caldas, L.K. Norford. Genetic algorithms for optimization of building envelopes and the design and control of HVAC systems. Journal of Solar Energy Engineering 125 (3) (2003) 343-351. doi:10.1115/1.1591803.

[34] W. Wang, R. Zmeureanu, H. Rivard. Applying multi-objective genetic algorithms in green building design optimization. Building and Environment 40 (11) (2005) 1512-1525. https://doi.org/10.1016/j.buildenv.2004.11.017.

[35] S.A. Klein, W.A. Beckman, J.W. Mitchell, J.A. Duffie, N.A. Duffie, T.L.Freeman, J.C.Mitchell, J.E. Braun, B.L.Evans, J.P. Kummer, R.E. Urban, A. Fikesel, J.W. Thornton, N.J.Blair, P.M.Williams, D.E. Bradley, T.P.McDowell, M.Kumment, D.A. Arias. TRNSYS, a Transient Simulation Program, 2006. (University of Wisconsin-Madison, USA: Solar Energy Laboratory, Version 16). http://web.mit.edu/parmstr/Public/Documentation/08-ProgrammersGuide.pdf (last viewed date: July 2, 2018).